Supplementary Information towards:

BILP-19—An Ultramicroporous Organic Network with Exceptional Carbon Dioxide Uptake

Christoph Klumpen [1], Florian Radakovitsch [2], Andreas Jess [2] and Jürgen Senker [1,*]

[1] Inorganic Chemistry III, University of Bayreuth, Universitätsstraße 30, 95440 Bayreuth, Germany; christoph.klumpen@uni-bayreuth.de
[2] Chair of Chemical Engineering, University of Bayreuth, Universitätsstraße 30, 95440 Bayreuth, Germany; florian.radakovitsch@uni-bayreuth.de (F.R.); jess@uni-bayreuth.de (A.J.)
* Correspondence: juergen.senker@uni-bayreuth.de; Tel.: +49-(0)921-552532

Table of Content

1. General Information

1.1 Literature on Benzimidazole linked Polymers (BILPs)

Table S1: Key values of literature known porous polybenzimidazoles. For "?" assigned networks no literature could be found.

Network	S_A (BET) / $m^2 \cdot g^{-1}$	CO_2_273K / $mmol \cdot g^{-1}$	CO_2/N_2 // 273K Henry	CO_2/CH_4 // 273 K Henry
BILP-1[1]	1172 ^{Ar}	4.27	70	10
BILP-2[2]	708 ^{Ar}	3.39	113	17
BILP-3[3]	1306 ^{Ar}	5.11	59	8
BILP-4[2]	1135 ^{Ar}	5.34	79	10
BILP-5[2]	599 ^{Ar}	2.91	95	10
BILP-6[3]	1261 ^{Ar}	4.79	63	8
BILP-7[2]	1122 ^{Ar}	4.39	62	9
BILP-8[?]	-	-	-	-
BILP-9[?]	-	-	-	-
BILP-10[4]	787^{Ar}	4.02	111	14
BILP-11[4]	658 ^{Ar}	3.09	103	11
BILP-12[4]	1497 ^{Ar}	5.07	56	8
BILP-13[4]	677 ^{Ar}	2.57	103	9
BILP-14[?]	-	-	-	-
BILP-15[5]	448 ^{Ar}	2.68	83	9
BILP-16[5]	435 ^{Ar}	2.70	53	10
BILP-15(AC) [5]	862 ^{Ar}	3.43	61	9
BILP-16(AC) [5]	643 ^{Ar}	3.45	49	9
BILP-17[6]	952 ^{Ar}	-	-	-
BILP-18[6]	947 ^{Ar}	-	-	-
BILP-101[7]	536^{N2}	2.43^{298K}	80	-
PPN-101[8]	1096^{N2}	5.14	199 IAST	-
TBILP-1[9]	330^{Ar}	117 mg/g	63	9
TBILP-2[9]	1080^{Ar}	228 mg/g	40	7

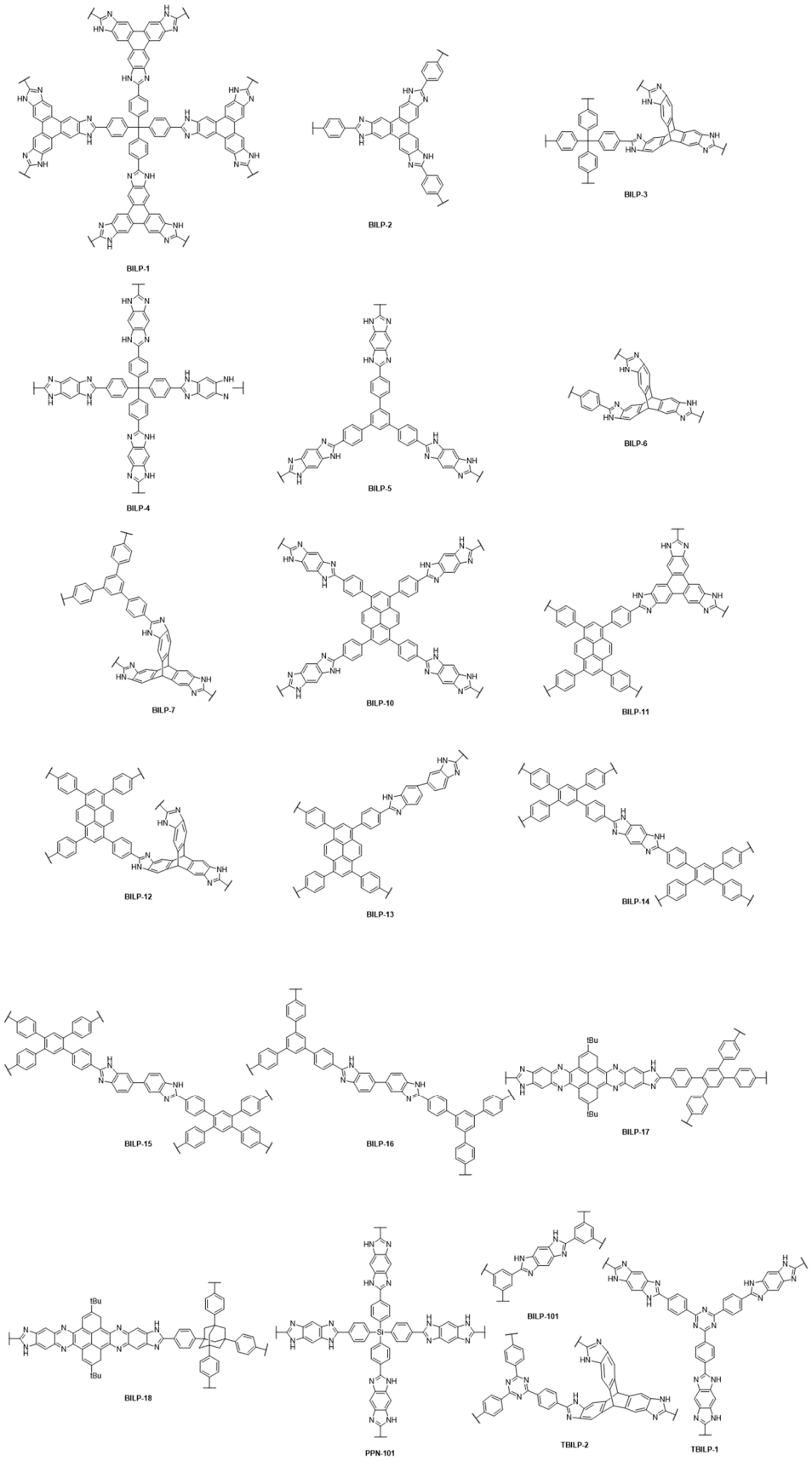

Figure S1: Schematic presentation of the benzimidazole based porous polymers compared in Table S1.

2. Characterization

2.1 Infrared Spectroscopy (IR)

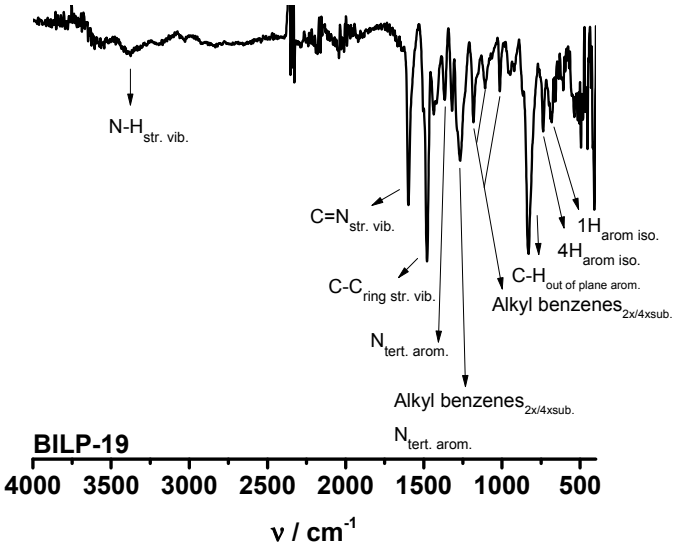

Figure S2: Infrared spectrum of BILP-19 and assignment of the most characteristic signals.

2.2 Powder X-ray diffraction (PXRD)

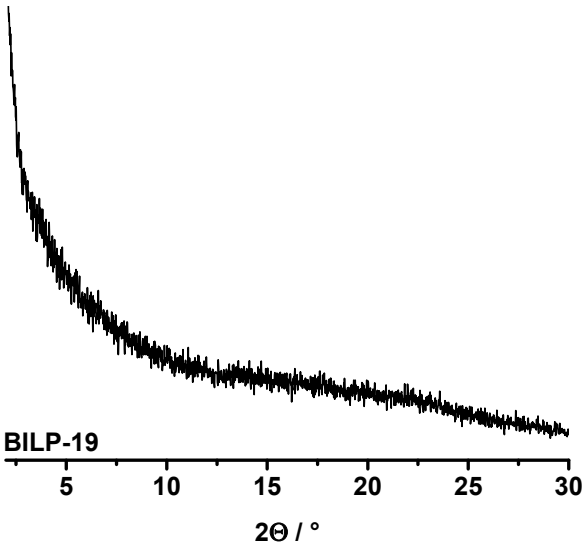

Figure S3: PXRD diffractogram of BILP-19.

2.3 Thermogravimetric analysis (TGA)

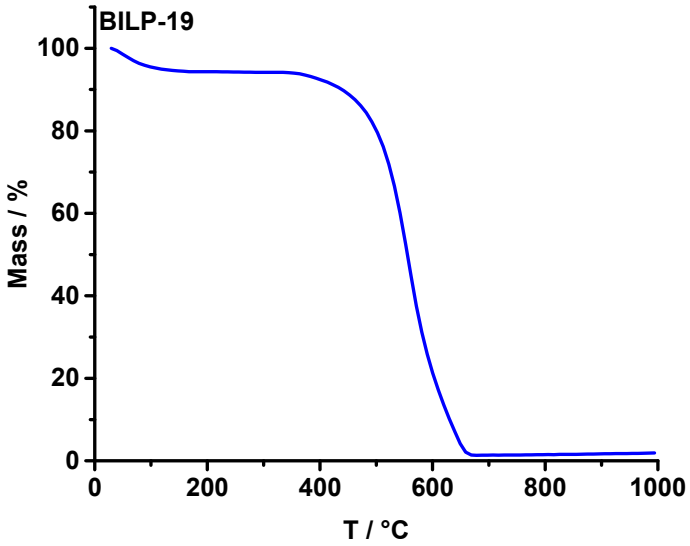

Figure S4: TGA curve of BILP-19 measured under air.

2.4 Scanning Electron Microscopy (SEM)

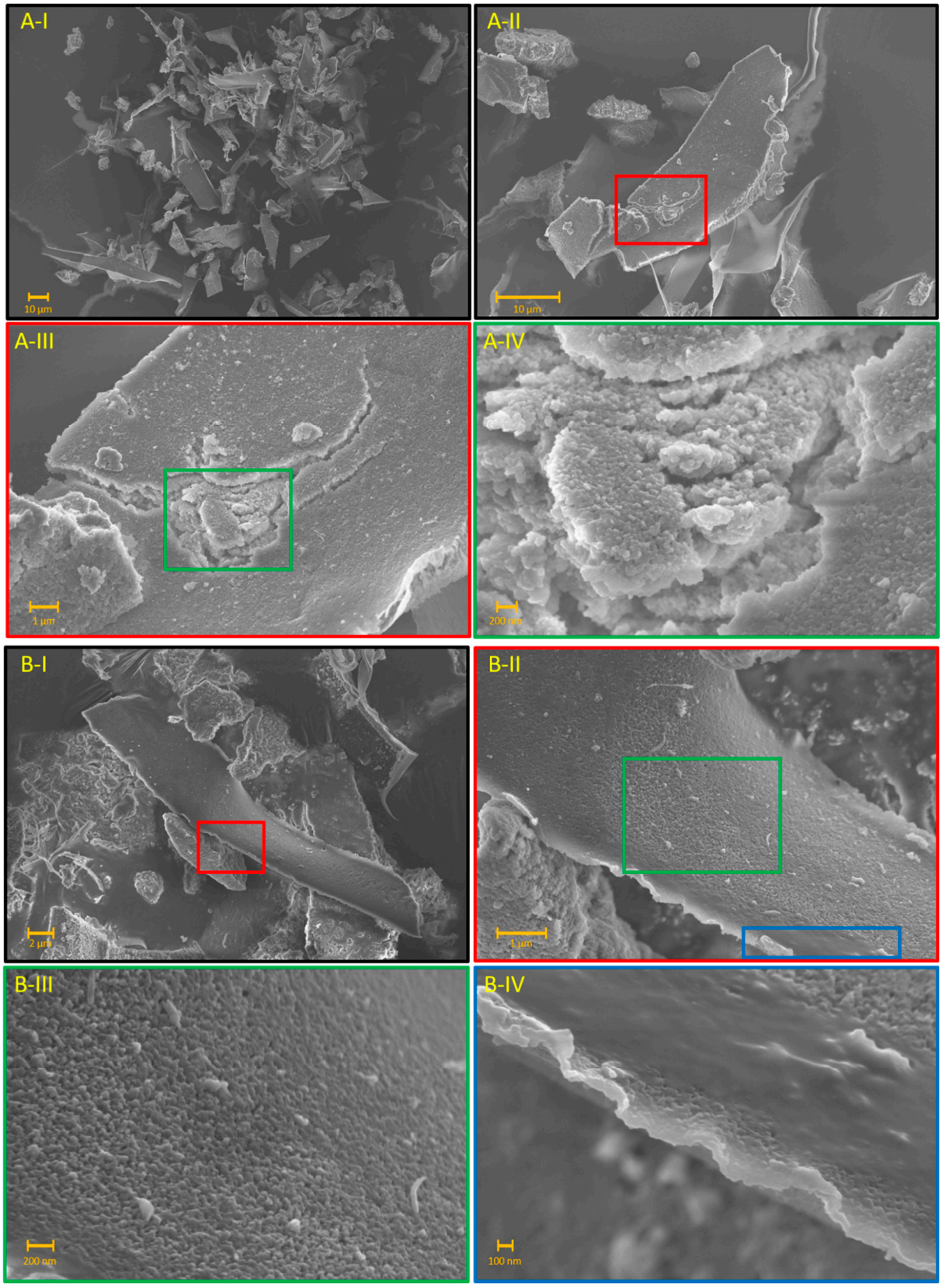

Figure S5: SEM Images of BILP-19, taken at to different positions (A, B).

2.5 Nuclear Magnetic Resonance (NMR)

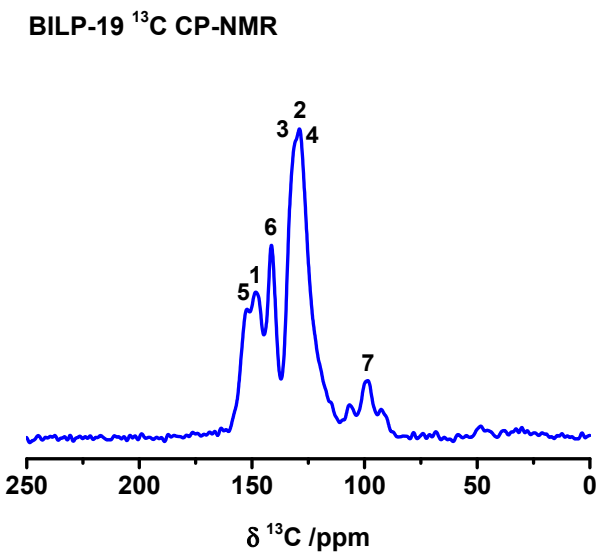

Figure S6: Complete ^{13}C MAS CP NMR spectrum of BILP-19.

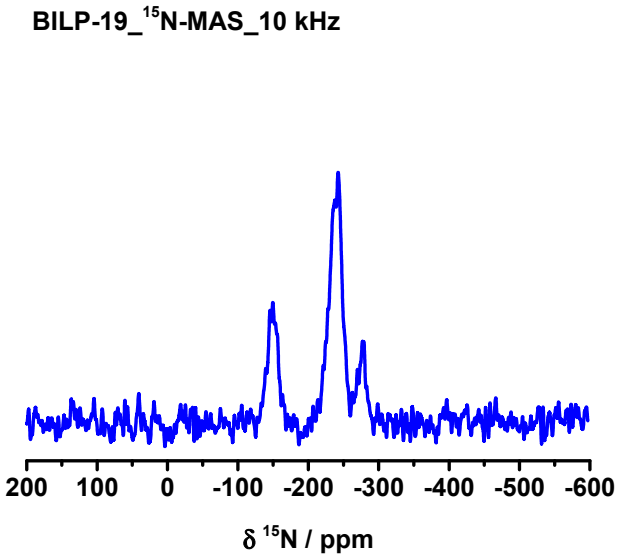

Figure S7: Complete ^{15}N CP MAS NMR spectrum of BILP-19.

2.6 Surface area and porosity

Table S2: Surface area and porosity of BILP-19 estimated from Ar, N_2 and CO_2 sorption isotherms, respectively.

Adsorbtive	S_{A_BET} / $m^2 \cdot g^{-1}$	S_{A_DFT} / $m^2 \cdot g^{-1}$	$P_{V\_tot.}$ / $cm^3 \cdot g^{-1}$	$P_{V\_mic.}$ / $cm^3 \cdot g^{-1}$	$P_{V\_mic.}$ / $P_{V\_tot.}$
Ar	144	128	0.0232	0.013	0.04
N_2	252	227	0.382	0.035	0.09
CO_2	-	1325	0.442	-	-

2.7 CHN analysis

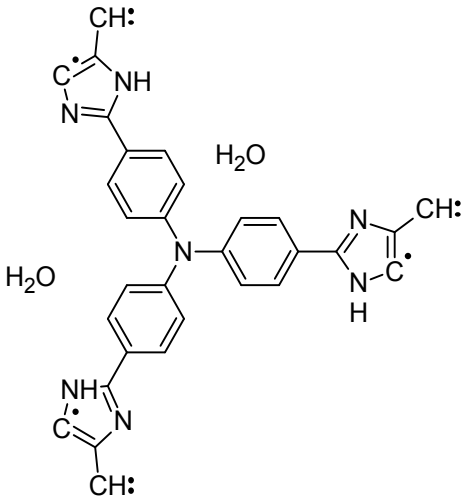

Table S3: Results of CHN analysis of BILP-19. Due to water content of 6 %, obtained by thermogravimetric analysis, two water molecules per linker were included in the theoretical calculations.

	C / %	H / %	N / %
BILP-19·2H$_2$O$_{meas.}$	65.67	4.24	17.94
BILP-19·2H$_2$O$_{calc.}$	70.30	4.33	19.13
Deviation	4.63	0.09	1.19

3. Gas Sorption and Selectivity

3.1 Carbon dioxide

3.1.1 Isosteric heat of adsorption

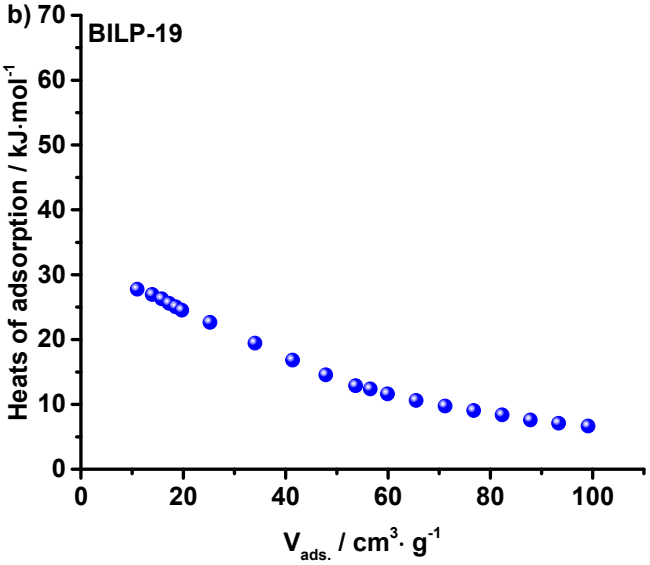

Figure S8: Isosteric heats of adsorption calculated from carbon dioxide adsorption isotherms measured at 273 K, 298 K and 313 K.

3.1.1 CO_2_Henry

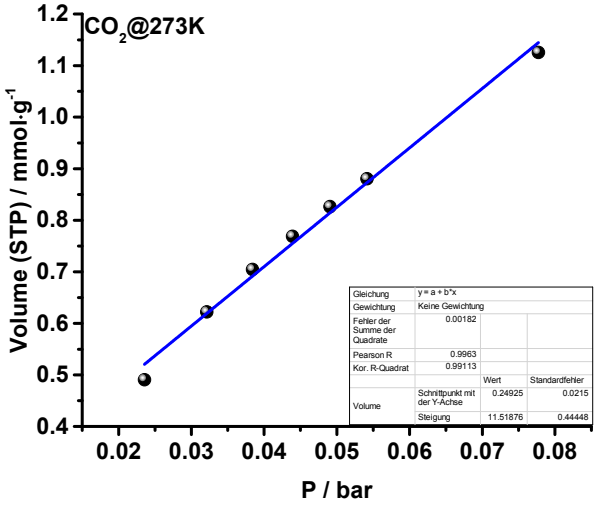

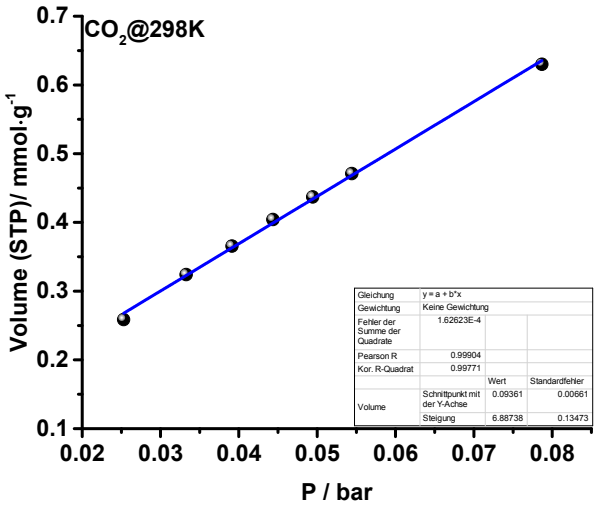

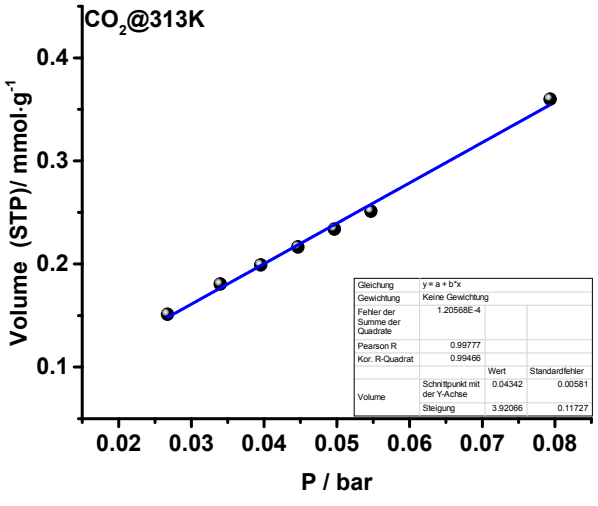

Figure S9: Fits for initial slope calculations (Henry method) of CO_2 isotherms measured at 273, 298 and 313 K.

3.1.2 CO_2_IAST

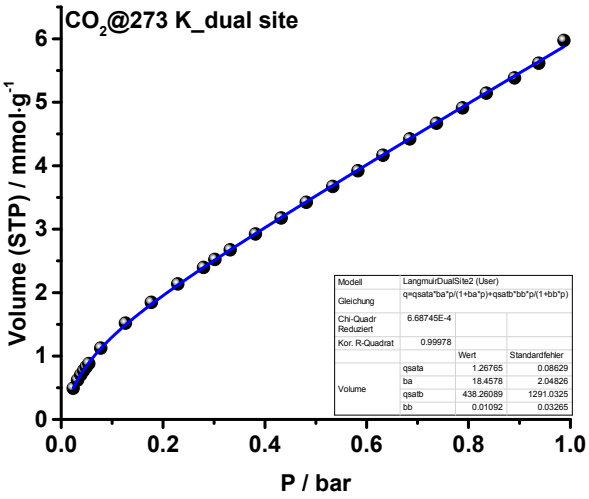

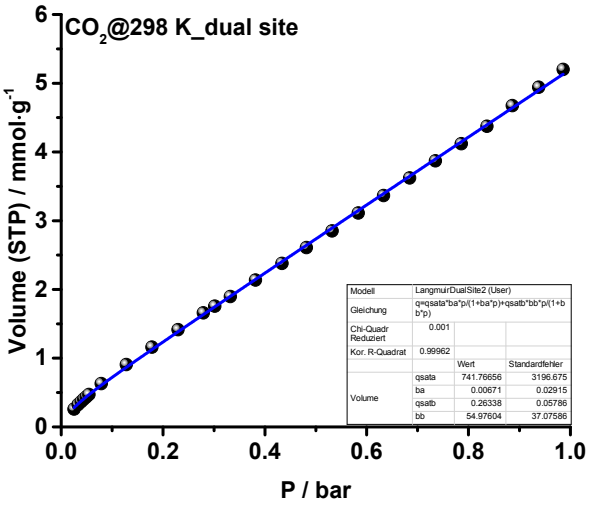

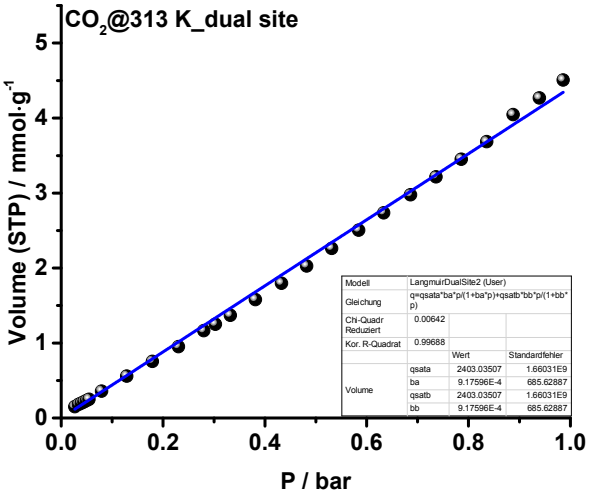

Figure S10: Langmuir dual site fits for CO_2 adsorption isotherms measured at 273, 298 and 313 K.

3.2 Nitrogen

3.2.1 Adsorption

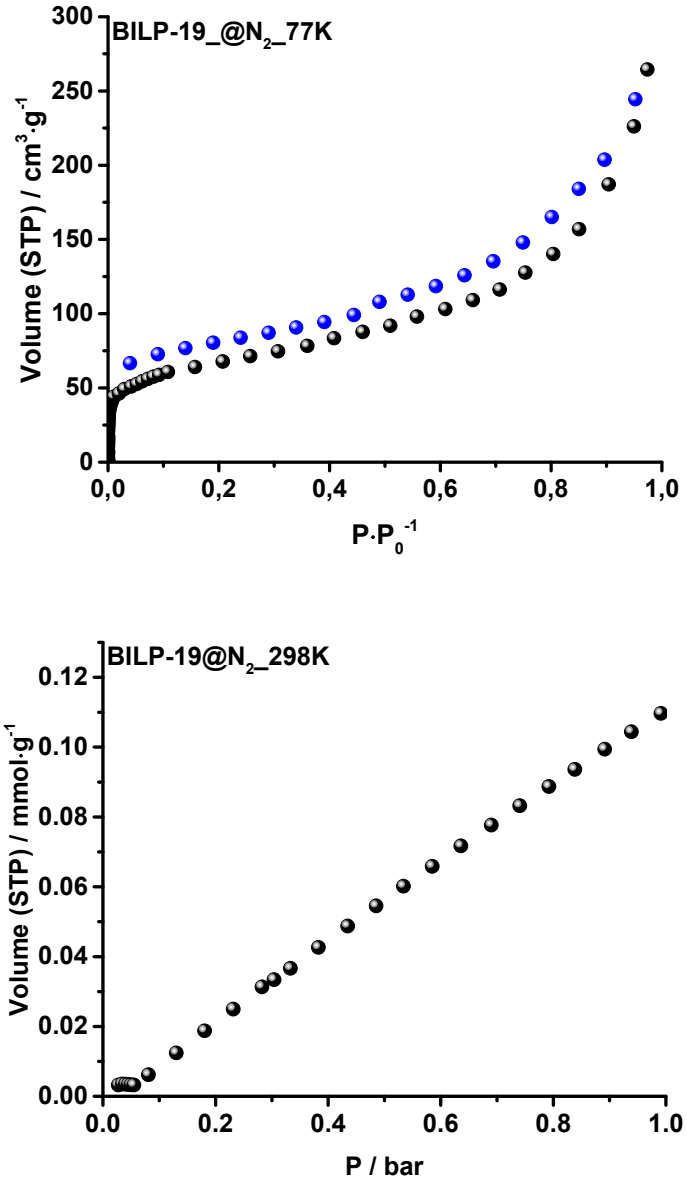

Figure S11: Nitrogen adsorption isotherm measured at 77K (top) and 298 K (bottom).

3.2.2 N_2 Henry

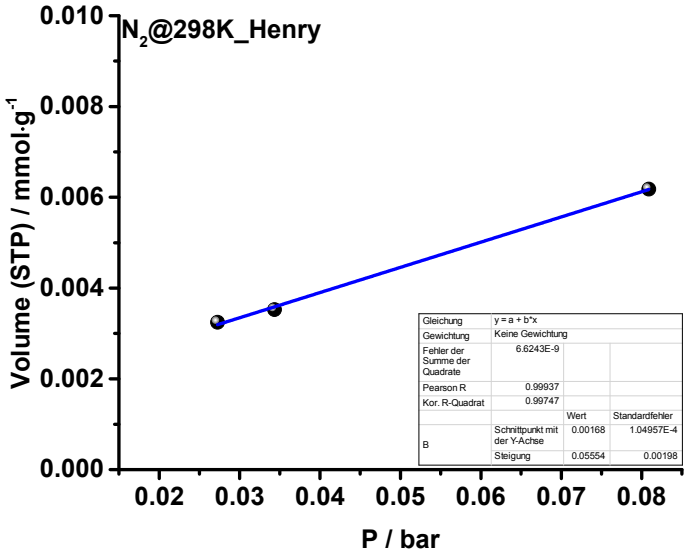

Figure S12: Initial slope of pure component fit for nitrogen adsorption at 298 K.

3.2.3 N_2 IAST

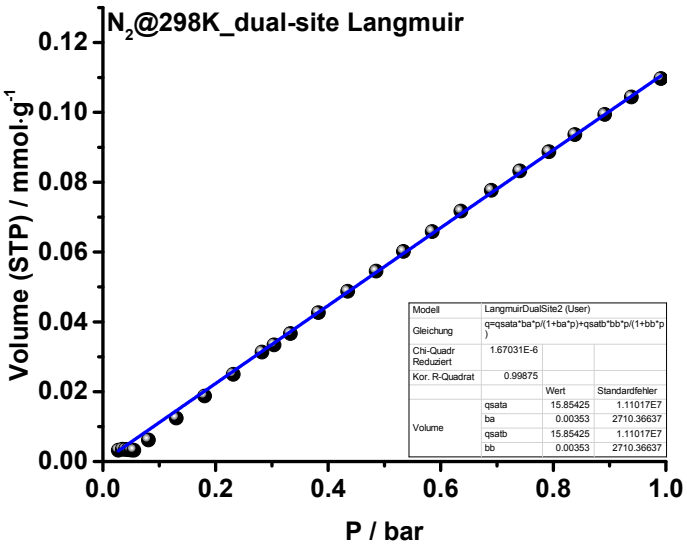

Figure S13: Langmuir dual site fit of N_2 sorption isotherms measured at 298 K.

3.3 Methane

3.3.1 Henry

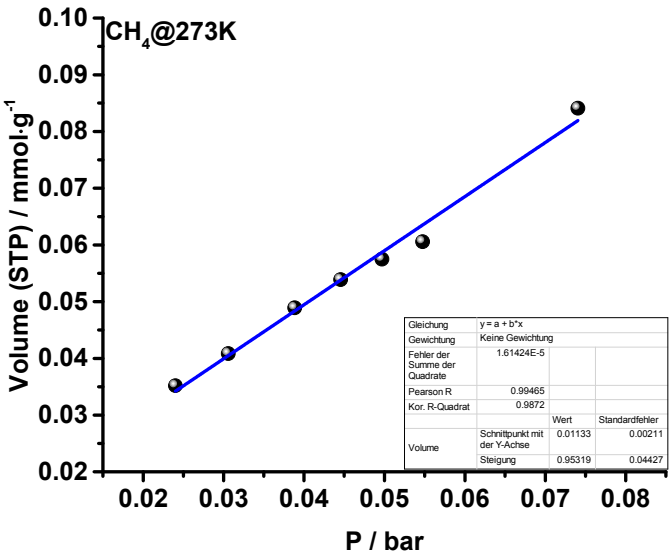

Figure S14: Initial slope of pure component adsorption fit for CH_4, measured at 273 K.

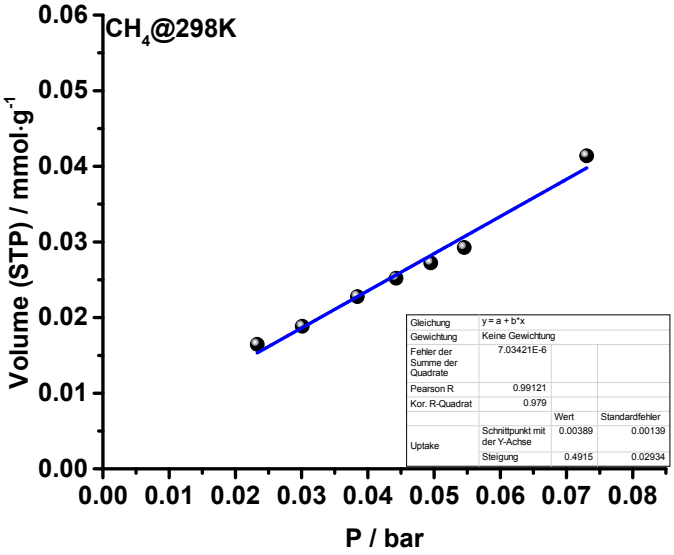

Figure S15: Initial slope of pure component adsorption fit for CH_4, measured at 298 K.

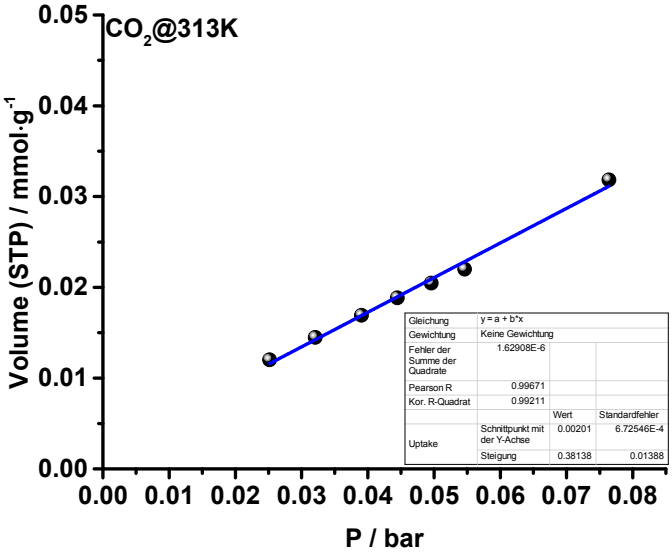

Figure S16: Initial slope of pure component adsorption fit for CH_4, measured at 313 K.

3.3.2 IAST

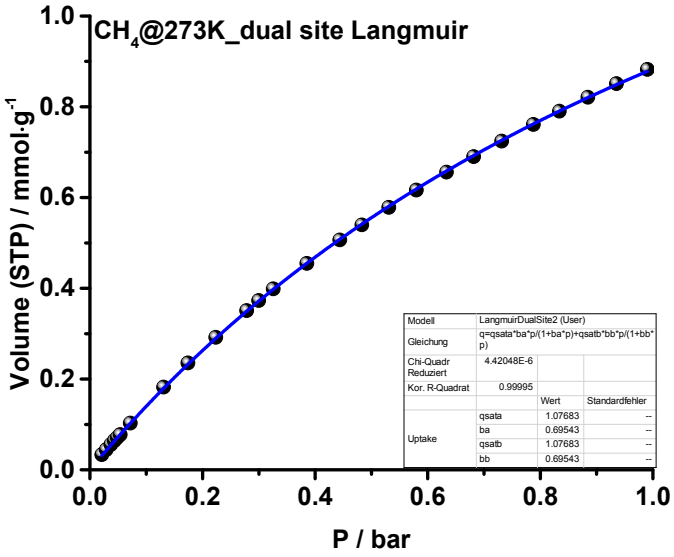

Figure S17: Langmuir dual site fit of CH_4 sorption isotherms measured at 298 K.

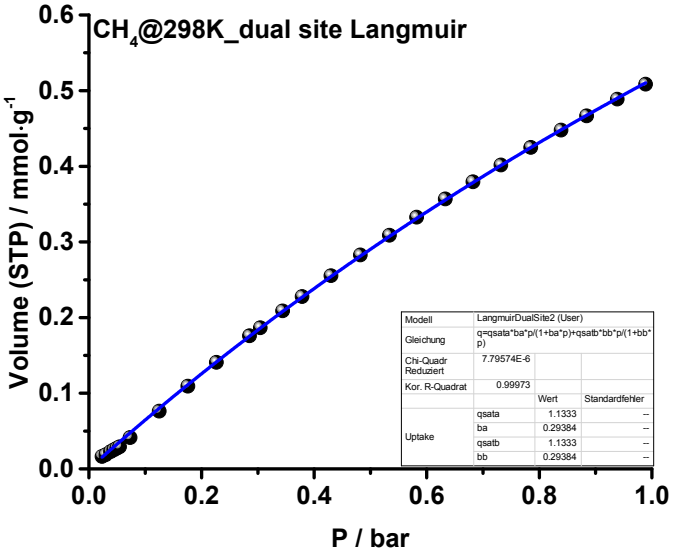

Figure S18: Langmuir dual site fit of CH_4 sorption isotherms measured at 298 K.

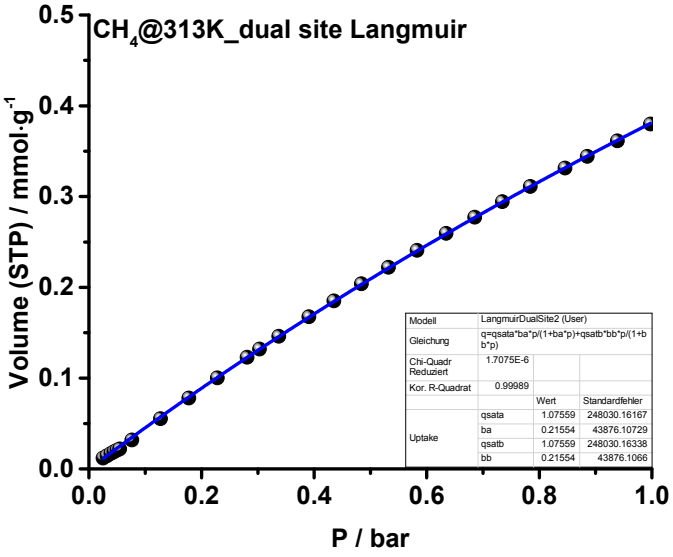

Figure S19: Langmuir dual site fit of CH_4 sorption isotherms measured at 313 K.

3.4 Argon

3.4.1 T-Plot

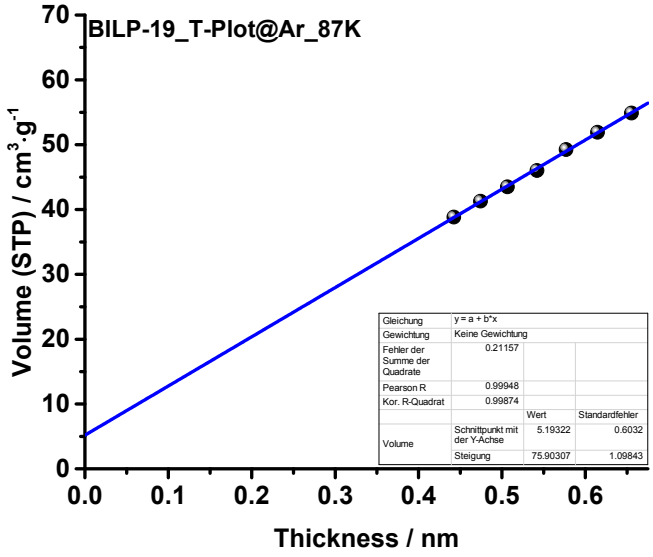

Figure S20: T-Plot applied on Ar isotherm measured at 87 K. The P/P0 range was 0.2 - 0.5.

3.5 Selectivities based on IAST calculations

3.5.1 Carbon dioxide over nitrogen

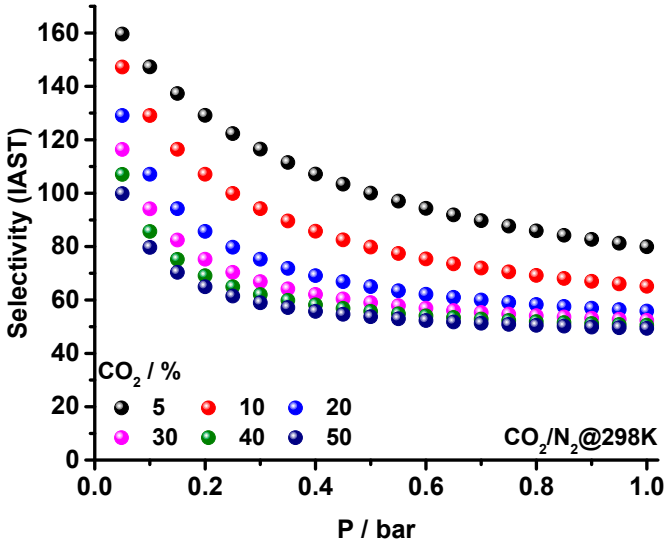

Figure S21: Selectivities of carbon dioxide over nitrogen, based on IAST calculations for different contents of carbon dioxide at 298 K.

3.5.2 Carbon dioxide over methane

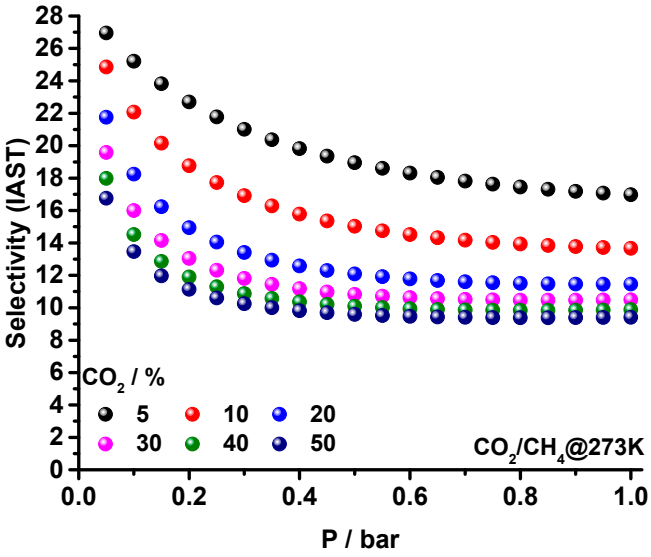

Figure S22: Selectivities of carbon dioxide over methane, based on IAST calculations for different contents of carbon dioxide at 273 K.

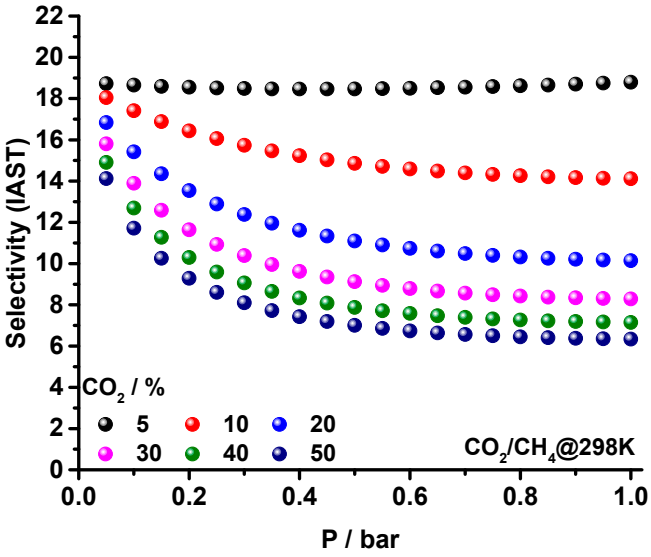

Figure S23: Selectivities of carbon dioxide over methane, based on IAST calculations for different contents of carbon dioxide at 298 K.

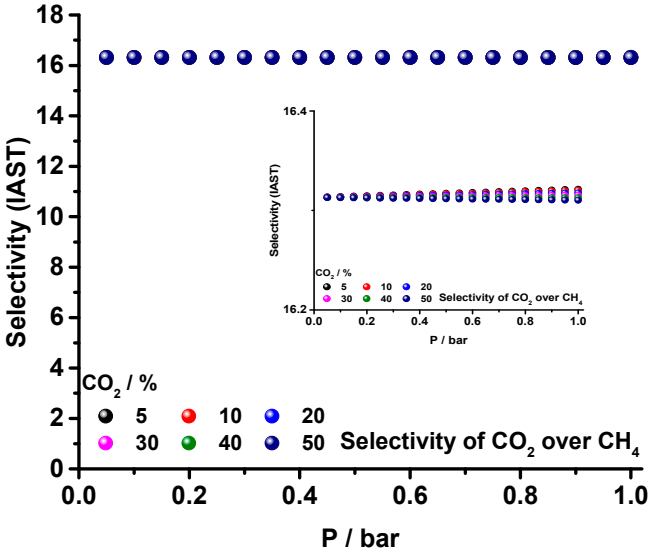

Figure S24: Selectivities of carbon dioxide over methane, based on IAST calculations for different contents of carbon dioxide at 313 K.

4. Literature

1. Rabbani, M. G.; El-Kaderi, H. M. Template-Free Synthesis of a Highly Porous Benzimidazole-Linked Polymer for CO_2 Capture and H2 Storage. *Chem. Mater.* **2011**, *23*, 1650–1653.

2. Rabbani, M. G.; El-Kaderi, H. M. Synthesis and Characterization of Porous Benzimidazole-Linked Polymers and Their Performance in Small Gas Storage and Selective Uptake. *Chem. Mater.* **2012**, *24*, 1511–1517.

3. Rabbani, M. G.; Reich, T. E.; Kassab, R. M.; Jackson, K. T.; El-Kaderi, H. M. High CO_2 uptake and selectivity by triptycene-derived benzimidazole-linked polymers. *Chem. Commun.* **2012**, *48*, 1141–1143.

4. Sekizkardes, A. K.; İslamoğlu, T.; Kahveci, Z.; El-Kaderi, H. M. Application of pyrene-derived benzimidazole-linked polymers to CO_2 separation under pressure and vacuum swing adsorption settings. *J. Mater. Chem. A* **2014**, *2*, 12492.

5. Altarawneh, S.; İslamoğlu, T.; Sekizkardes, A. K.; El-Kaderi, H. M. Effect of Acid-Catalyzed Formation Rates of Benzimidazole-Linked Polymers on Porosity and Selective CO_2 Capture from Gas Mixtures. *Environ. Sci. Technol.* **2015**, *49*, 4715–4723.

6. Altarawneh, S.; Nahar, L.; Arachchige, I. U.; El-Ballouli, A. O.; Hallal, K. M.; Kaafarani, B. R.; Rabbani, M. G.; Arvapally, R. K.; El-Kaderi, H. M. Highly porous and photoluminescent pyrene-quinoxaline-derived benzimidazole-linked polymers. *J. Mater. Chem. A* **2015**, *3*, 3006–3010.

7. Sekizkardes, A. K.; Culp, J. T.; Islamoglu, T.; Marti, A.; Hopkinson, D.; Myers, C.; El-Kaderi, H. M.; Nulwala, H. B. An ultra-microporous organic polymer for high performance carbon dioxide capture and separation. *Chem. Commun. Chem. Commun* **2015**, *51*, 13393–13396.

8. Zhang, M.; Perry, Z.; Park, J.; Zhou, H.-C. Stable benzimidazole-incorporated porous polymer network for carbon capture with high efficiency and low cost. *Polymer (Guildf).* **2014**, *55*, 335–339.

9. Sekizkardes, A. K.; Altarawneh, S.; Kahveci, Z.; Islamo◎lu, T.; El-Kaderi, H. M. Highly selective CO_2 capture by triazine-based benzimidazole-linked polymers. *Macromolecules* **2014**, *47*, 8328–8334.